(Received 29 February 2024, Accepted 16 April 2024, Scheduled 24 April 2024)

Research on Electromagnetic Vibration and Noise Suppression of PMaSynRM with Slotted Stator and Rotor

Zhentian Zhu*, Aiyuan Wang, and Ming Tang

School of Electrical Engineering, Shanghai Dianji University, Shanghai 201306, China

ABSTRACT: Permanent magnet assisted synchronous reluctance motor (PMaSynRM) has been widely concerned, but the research on the vibration and noise of this kind of motor is relatively limited. In addressing the problem of significant vibration noise caused by radial electromagnetic force waves in PMaSynRM, the research explored a motor vibration and noise suppression solution involving stator slotting and rotor magnetic isolation hole opening. The study analyzed the impact of different slotting parameters on the radial electromagnetic force and air gap magnetic flux density of the motor and compared it with the solution involving slotting of the stator teeth only and magnetic isolation hole opening of the rotor only. Finally, the modal, vibration response, and noise response of the motor after slotting are analyzed and verified. The results show that the amplitude of radial electromagnetic force and the total harmonic distortion rate of the air gap magnetic flux density of the motor are significantly reduced by opening the stator auxiliary slot and rotor magnetic isolation hole. The maximum vibration acceleration of the motor is reduced by 33.44 mm/s^2, and the peak A-weighted sound pressure level of the motor decreases by 5.68 dBA.

1. INTRODUCTION

Permanent magnet assisted synchronous reluctance motors, with advantages such as low dependence on rare earth materials, wide speed range, low cost, and high drive efficiency, are currently widely used in engineering fields such as new energy vehicles, compressors, and robots [1–3]. However, its complex rotor magnetic circuit structure and high saliency ratio lead to increased radial electromagnetic force amplitude due to high air gap magnetic density harmonics, resulting in significant vibration and noise issues [4, 5]. This affects the smooth operation and lifespan of the motor, especially considering the stringent requirements for vibration and noise in new energy vehicles. Therefore, effectively suppressing the electromagnetic vibration and noise issues in PMaSynRM is of great significance and research value.

Ref. [6] suppresses motor vibration and noise by altering the pole arc coefficient and magnetic pole eccentricity. Ref. [7] suggests that changing the damping of materials can effectively reduce the high-frequency vibration response of the motor, lowering the amplitude of motor vibration acceleration. Ref. [8] modifies the shape of permanent magnets and rotor core surface to optimize the reduction of air gap magnetic density harmonics, thereby reducing motor vibration. Ref. [9] optimizes a rotor demagnetization bridge structure, altering the electromagnetic excitation force on the motor stator teeth to decrease motor vibration and noise. Ref. [10] analyzes the motor's vibration characteristics in terms of pole groove coordination and shell material. Ref. [11] adopts the method of slotting the top of motor stator teeth to improve motor vibration and noise. Ref. [12] investigates the impact of factors such as the number of magnetic steel layers in the built-in motor rotor, the angle cutting of magnetic steel ends, and demagnetization holes on motor vibration and noise. Refs [13, 14] derive analytical expressions for radial electromagnetic force waves in the motor after segmented skewed rotor and analyze the suppression mechanism of segmented skewed rotor on electromagnetic vibration and noise in permanent magnet synchronous motors. In addition to the optimization of the motor's geometric structure mentioned above, other methods mainly concern the influence of current excitation on the electromagnetic vibration and noise of the motor. Ref. [15] analyzes the impact of current harmonics generated during the operation of the inverter on the motor's electromagnetic noise. Ref. [16] focuses on reducing the electromagnetic vibration and noise of the motor by suppressing the amplitude of current harmonics in the inverter. Ref. [17] studies vibration and noise under different power supply currents, explaining the characteristics of changes in noise and vibration peaks through variations in the amplitude of the lowest spatial force wave caused by current harmonics.

Based on the above research, this paper takes a 132 kW H315 frame number PMaSynRM as the research object from the perspective of motor body structure design. The vibration and noise of the motor are suppressed by the scheme of opening auxiliary slots in stator teeth and opening magnetic holes in rotor. The corresponding finite element simulation model is built, and the influence of different slotting parameters of stator and rotor on radial electromagnetic force and air gap flux density is analyzed. Finally, the feasibility of this scheme is verified by multi-physical field simulation of modal, harmonic response, and acoustic response. While ensuring that other electromagnetic performance is almost not lost, the purpose of effectively

* Corresponding author: Zhentian Zhu (648457429@qq.com).

suppressing the electromagnetic vibration and noise of the motor is achieved, which has certain reference significance and application value.

2. THE PRINCIPLE OF ELECTROMAGNETIC VIBRATION AND NOISE

When the motor is running, the interaction of magnetic fields in the air gap between stator and rotor generates radial electromagnetic forces that vary with time and space on the stator core. This causes the motor to undergo periodic vibrations and radiate electromagnetic noise, which is the main reason for motor vibration noise. According to the Maxwell Tensor method, the radial electromagnetic force on the inner surface of the stator can be expressed as:

$$F_r(\theta,t) = \frac{b_r^2(\theta,t) - b_t^2(\theta,t)}{2\mu_0} \tag{1}$$

where θ represents the spatial position angle of the rotor; t represents time; μ_0 represents the vacuum permeability; $b_r(\theta,t)$ represents the radial air gap magnetic flux density; $b_t(\theta,t)$ represents the tangential air gap magnetic flux density.

Since the permeability of air is much smaller than the permeability of the core material, the magnetic field lines in the air gap are approximately perpendicular to the center arc. Therefore, the tangential air gap magnetic flux density is much smaller than the radial air gap magnetic flux density and can be neglected. The radial electromagnetic force can be simplified as:

$$F_r(\theta,t) = \frac{b_r^2(\theta,t)}{2\mu_0} \tag{2}$$

The magnetic field generated by the rotor permanent magnet interacts with the magnetic field generated by the stator winding. The magnetic potential harmonics generated by the rotor permanent magnet and the stator winding are as follows:

$$u = 2a + 1 \tag{3}$$

$$v = \frac{6b}{d} + 1 \tag{4}$$

where $a = 0, 1, 2, 3, \ldots$; $b = 0, \pm1, \pm2, \pm3, \ldots$; d is the denominator of the number of slots per pole and per phase. The number of slots per pole and per phase of the motor involved in this paper is 3/2, so d takes 2 in this paper.

The order of electromagnetic force and the corresponding frequency of electromagnetic force under each harmonic of the motor are expressed as:

$$m = (u \pm v)\, p \tag{5}$$

$$f_r = (1 \pm u)\, f \tag{6}$$

where p is the number of poles of the motor; f is the fundamental frequency of the motor.

The vibration amplitude of the motor is proportional to the amplitude of the radial electromagnetic force of the motor, which can be expressed as:

$$A \propto \frac{F_r}{K m^4} \tag{7}$$

where A represents the amplitude of vibration acceleration; F_r represents the amplitude of radial electromagnetic force; K is the vibration coefficient.

Considering the effect of motor slotting, the air gap permeance function and the air gap magnetic flux density expression are respectively as follows:

$$\Lambda(\theta,t) = \Lambda_0 + \sum_{k=1,2,3\cdots} \Lambda_k \cos(kp\theta - k\omega t) \tag{8}$$

$$b_r(\theta t) = \sum F_\mu \Lambda_0 \cos(\mu\omega t - \mu p\theta) + \sum \frac{1}{2} F_\mu \Lambda_k \cos[\mu\omega t - (\mu p \pm kZ)\theta] \tag{9}$$

where Λ_0 represents the direct current component of magnetic flux linkage; Λ_k represents the amplitude of k-th order magnetic flux harmonics; Z stands for the number of slots in the motor; F_μ represents the magnetomotive force; μ is the amplitude of subharmonics; ω is fundamental angular frequency.

3. STRUCTURE AND MAIN PARAMETERS

The study focuses on the investigation of an H315 frame size ferrite permanent magnet assisted synchronous reluctance motor. The motor employs a 72-slot 16-pole slot-pole combination, with a stator winding form of short-pitch double-layer winding and a rotor utilizing a double-layer U-shaped topology. The 2D finite element model of the motor is illustrated in Figure 1, with its key parameters listed in Table 1.

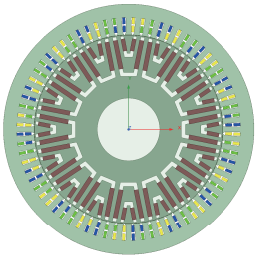

FIGURE 1. The finite element cross-sectional model of PMaSynRM.

TABLE 1. Main parameters of PMaSynRM.

Rated power/kW	132
Rated speed/rpm	1500
Rated voltage/V	380
Rated current/A	239.5
Stator outer diameter/mm	520
Stator inner diameter/mm	393
Gap length/mm	1
Rotor inner diameter/mm	130
Permanent magnet brand	Y30BH

4. DESIGN AND ANALYSIS OF SLOTTING OF PMASYNRM

The stator tooth auxiliary slot is shown in Figure 2(a). The stator slotting method adopts rectangular slots opened at the cen-

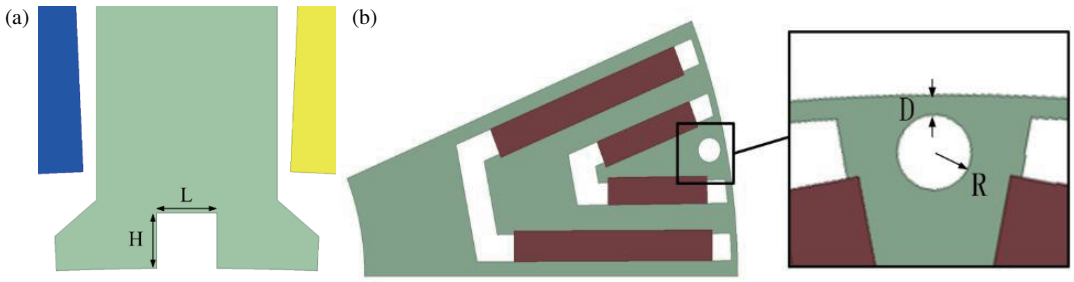

FIGURE 2. (a) Auxiliary slot of stator teeth. (b) Magnetic isolation hole of rotor.

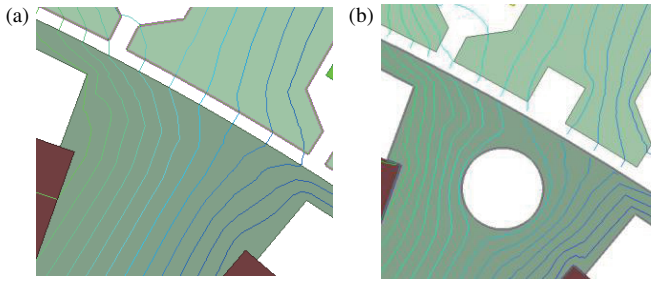

FIGURE 3. Comparison of magnetic lines before and after slotting. (a) Before slotting. (b) After slotting.

ter of the stator teeth. The depth of the stator auxiliary slot is represented by **H**, and the width of the stator auxiliary slot is represented by **L**. The rotor magnetic isolation hole is shown in Figure 2(b). In this paper, the isolation holes are circular openings, and the radius of the rotor magnetic isolation hole is represented by **R**. The distance between the isolation hole and air gap is represented by **D**. Compared with the auxiliary slots on the rotor, this structure has little impact on the magnetic reluctance of the motor air gap, thus having a smaller impact on torque performance.

The distributions of magnetic lines before and after slotting the stator and rotor of the motor are shown in Figure 3. The auxiliary slot of stator teeth makes the air gap length uneven, which corresponds to a certain reduction in radial air gap flux density, thus reducing the radial electromagnetic force. The opening of the rotor magnetic isolation hole leads to the inconsistency of the magnetic conductivity at this position, which leads to the decrease of the magnetic flux outlet angle, so that the radial component of the magnetic flux density is reduced, which is also conducive to reducing the radial electromagnetic force of the motor.

The value of each slotting parameter is evaluated by the two indexes of radial electromagnetic force amplitude (F_r) and air gap flux density total harmonic distortion (THD) rate. THD is a performance parameter representing the degree of waveform distortion in electrical related industries. The lower the THD is, the smaller the harmonic content is, the higher the stability of the motor is during operation, and the smaller the vibration and noise are generated. THD is expressed by the formula:

$$\mathrm{THD} = \frac{\sqrt{\sum_{n=2}^{\infty} B_n^2}}{B_1} \times 100\% \tag{10}$$

where n is the harmonic order, B_1 the amplitude of the fundamental wave of the air gap magnetic flux density, and B_n the nth harmonic amplitude of air gap magnetic flux density.

Due to the absence of coupling relationships between above parameters, this paper provides a detailed description of the parameters of the motor stator auxiliary slot and rotor isolation hole. While ensuring that the magnetic circuit is not saturated, the values of **L** range from 1 mm to 3.5 mm, **H** from 1 mm to 4 mm, **R** from 0.5mm to 3 mm, and **D** from 1 mm to 3 mm according to the structural dimensions of the motor. The influence of slot parameters of the stator and rotor on the amplitude of the radial electromagnetic force and the THD of the air gap magnetic flux density is shown in Figure 4.

With the increase of **L**, the radial electromagnetic force density decreases first, then increases slightly and then decreases continuously. When **L** reaches 3.5 mm, the radial electromagnetic force density reaches the minimum value of 428461 N/m^2. The THD of air gap flux density increases first and then decreases continuously. When **L** reaches 3.5 mm, the THD of air gap flux density reaches the minimum value of 17.4%. As **H** increases, the radial electromagnetic force density continues to decrease. When **H** reaches 4 mm, the radial electromagnetic force density takes the minimum value of 439402 N/m^2, but the air gap flux density THD first decreases to the minimum value of 18.2% and then continues to increase. Compared with the stator auxiliary slot, the rotor magnetic isolation hole has little influence on the radial electromagnetic force density of the air gap, but it has obvious influence on the THD of the air gap flux density. The influence of **R** on the radial electromagnetic force density of the air gap has no obvious change, but the THD shows a continuous downward trend, from 27.6% to 16.3%. With the increase of **D**, the radial electromagnetic force density increases slowly, and the harmonic distortion decreases

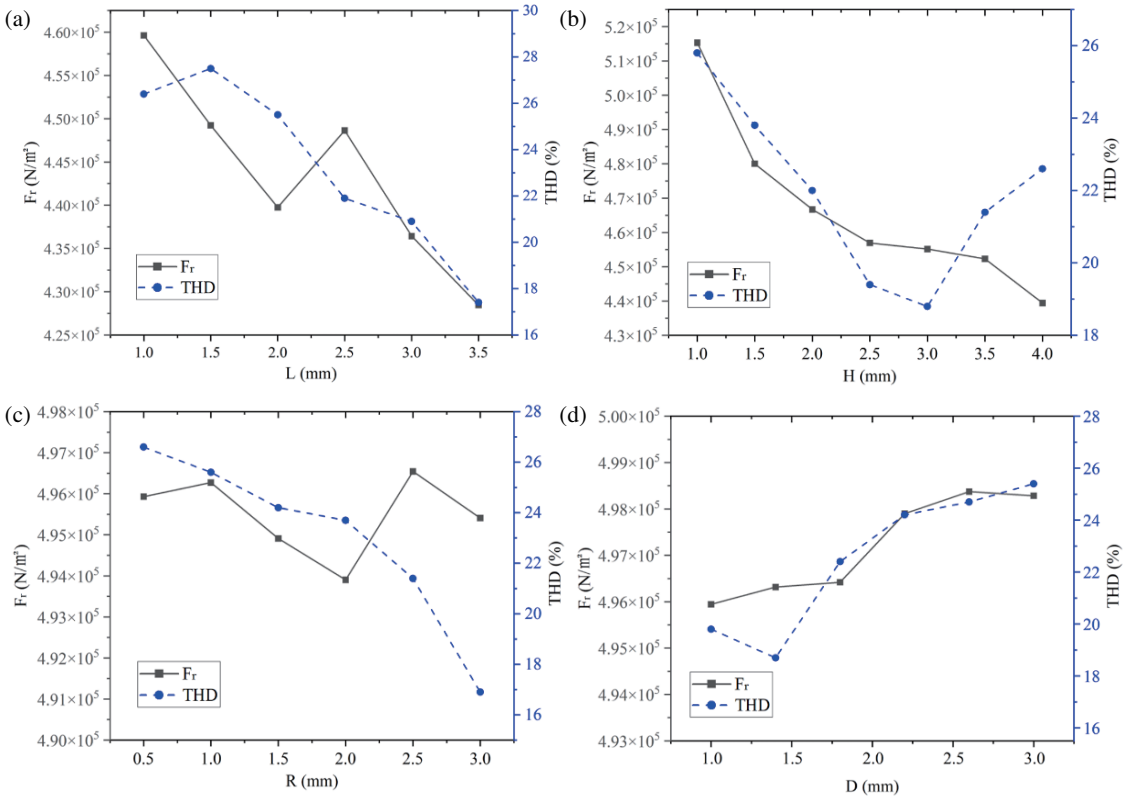

FIGURE 4. (a) The influence of stator auxiliary slot width. (b) The influence of stator auxiliary slot depth. (c) The influence of rotor magnetic isolation hole radius. (d) The influence of the distance between the rotor magnetic hole and the air gap distance.

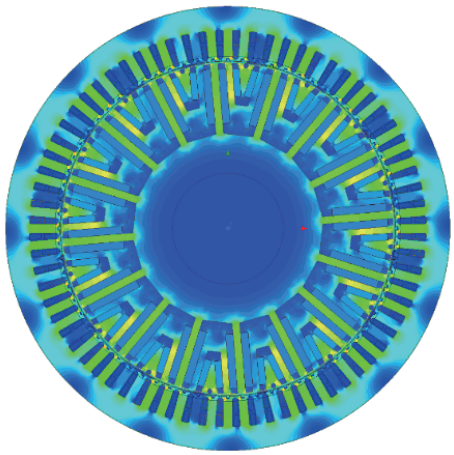

FIGURE 5. The magnetic dense cloud diagram of the motor after slotting.

first and then increases slowly, when **D** = 1.4 mm, the THD reaches the minimum value of 18.7%. Through comprehensive consideration, the value of **L** in this paper is 3.5 mm, the value of **H** 3 mm, the value of **R** 3 mm, and the value of **D** 1.4 mm.

Through the comparative analysis of Table 2, when only the stator auxiliary slots are opened, the weakening effect of the amplitude of the radial electromagnetic force density is better, but when only the rotor magnetic isolation holes are opened, the THD of the air gap flux density is smaller, and the opening of the stator auxiliary slots is combined with the opening of the rotor magnetic isolation holes. The weakening effect of the amplitude of the radial electromagnetic force density and the THD of the air gap flux density is the better than the first two, so this paper uses this scheme to optimize.

The motor is analyzed by ANSYS MAXWELL simulation software. Figure 5 shows the finite element magnetic density cloud diagram of the motor after slotting. The maximum magnetic flux density is measured to be 1.7 T, and the magnetic circuit is not saturated, which reflects the rationality of the magnetic circuit design.

TABLE 2. Comparison of slotting schemes.

Scheme	F_r (N/m^2)	THD (%)
Stator teeth slotting only	420504	19.77
Rotor magnetic isolation hole opening only	487097	18.45
Both of the above	395423	16.82

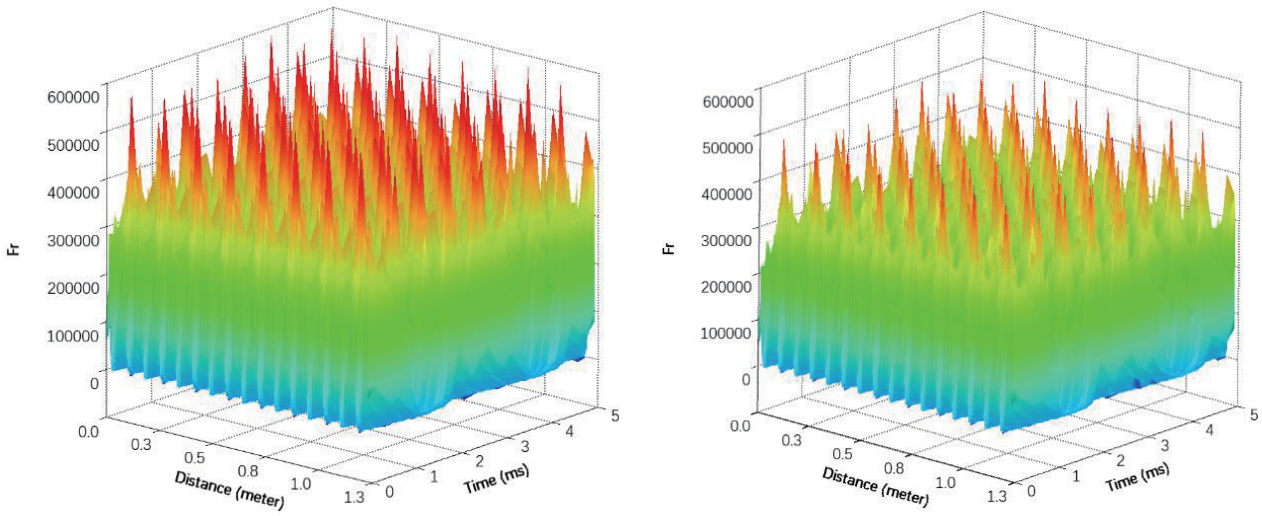

FIGURE 6. Space-time distribution of radial electromagnetic force.

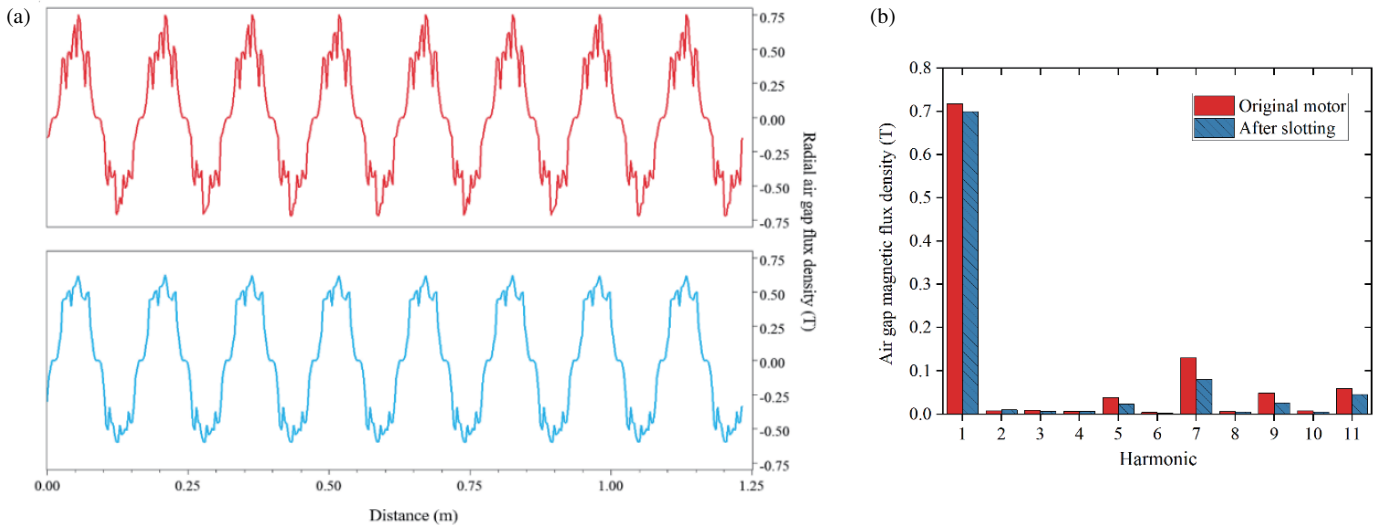

FIGURE 7. (a) Air gap flux density waveform. (b) Harmonic distribution of air gap flux density.

When the rotor undergoes rotational motion, the electromagnetic force possesses both temporal and spatial attributes when being observed from the entire circumference of the air gap. The radial electromagnetic force density is modified using the Maxwell Tensor method, and the transient field analysis is utilized to obtain the radial electromagnetic force simulation results of the motor. The temporal and spatial distributions of the radial electromagnetic force of the motor are shown in Figure 6. The original spatial-temporal distribution map of the radial electromagnetic force of the motor has many sharp peak waves, with a large amplitude of up to 559063 N/m^2. The amplitude of the spatial-temporal distribution of the radial electromagnetic force after slotting is 486585 N/m^2, which is 72478 N/m^2 lower than that of the original motor.

On the basis of the above electromagnetic force analysis, the radial air gap flux density of the motor in one electric cycle is further analyzed, and the air gap flux density waveform is decomposed by Fast Fourier Transform (FFT) to obtain the harmonic distribution of the air gap flux density. It can be seen from Figure 7(a) that the distortion of the air gap flux density

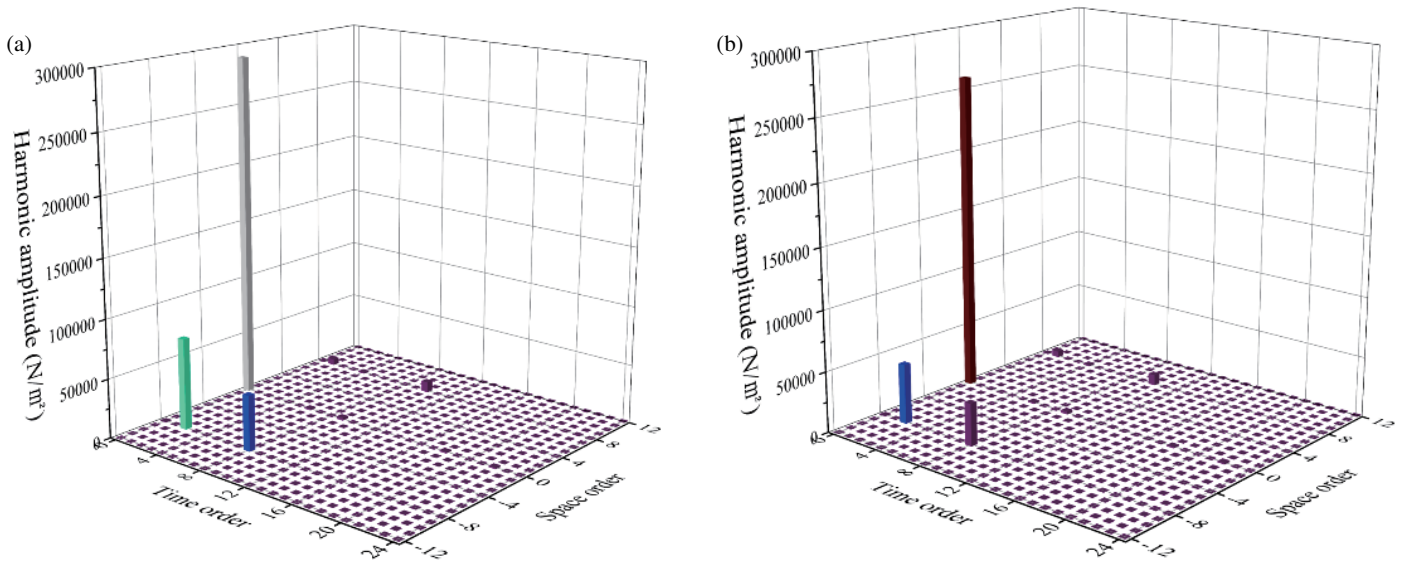

FIGURE 8. (a) The FFT space-time distribution of F_r of the original motor. (b) The FFT space-time distribution of F_r after slotting.

TABLE 3. Influence of other performance of PMaSynRM before and after slotting.

Performance	Before slotting	After slotting	Effect
Output torque (N·m)	840.2	835.8	↓ 4.4
Torque ripple (%)	20.5	18.1	↓ 2.4%
Electromagnetic efficiency (%)	97.41	97.55	↑ 0.14%
Power factor	0.877	0.892	↑ 0.015

waveform of the motor after the slotting design is reduced, and the sinusoidality is improved to some extent. Through the analysis of Figure 7(b), it can be seen that the 5rd, 7th, 9th, and 11th harmonics are lower than the original motor, which are reduced by 39.57%, 44.28%, 53.91%, and 20.25%, respectively. It can be seen that the effect of air gap flux density harmonic suppression after slotting design is better.

The FFT space-time distributions of the radial electromagnetic force of the motor before and after slotting are shown in Figure 8. It can be seen that the 2-order time, -8-order space and 8-order time, -8-order space of the original motor model will produce relatively large radial electromagnetic force harmonics. After slotting through the stator and rotor, the amplitude of the fundamental wave of the radial electromagnetic force decreases slightly. The 2-order time and -8-order space harmonics are reduced from 6.76×10^4 N/m^2 of the original motor to 4.28×10^4 N/m^2. The eighth-order time and-8-order space are reduced from the original 4.55×10^4 N/m^2 to 3.58×10^4 N/m^2. It can be seen that the harmonic component of the electromagnetic force is effectively weakened, which is beneficial to weaken the vibration and noise of the motor.

The electromagnetic performances of the motor before and after slotting are shown in Table 3. The output torque of the slotted motor is 835.8 N·m, which is slightly reduced by 4.4 N·m compared with the original motor. However, the torque ripple is reduced by 2.4% compared to the original motor, which makes the motor run more stable. At the same time, the efficiency and power factor of the slotted motor are 97.55% and 0.892, respectively, which are 0.14% and 0.015 higher than those of the original motor, so that the energy saving of the motor is guaranteed. Overall, the other performance of the motor almost did not suffer much loss.

5. VIBRATION AND NOISE ANALYSIS OF PMASYNRM

The simulation experiment is carried out with the help of Ansys Workbench platform, and the modal superposition method is adopted to calculate the surface vibration and noise response of the stator. Firstly, modal analysis is carried out on the structure of the stator, and then the simulation results of the electromagnetic force obtained from the finite element calculation are imported, and the excitation is set up to act on the teeth of the stator to carry out the harmonic response analysis. The electromagnetic force on the surface of the stator teeth is shown in Figure 9.

Since the electromagnetic force mainly acts on the circumferential plane of the stator, and the vibration of the motor mainly occurs on the stator, the radial mode of the stator is generally analyzed [18]. When the driving frequency of the motor is the same as the natural frequency of a certain mode of the motor stator, or when the stator vibration deformation caused by the radial electromagnetic force is the same as a certain natural mode, resonance phenomenon will occur, resulting in vibration and noise, affecting the normal operation and service life of the mo-

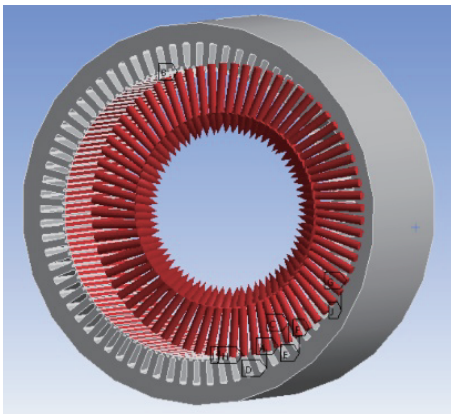

FIGURE 9. The electromagnetic force on the inner surface of the stator.

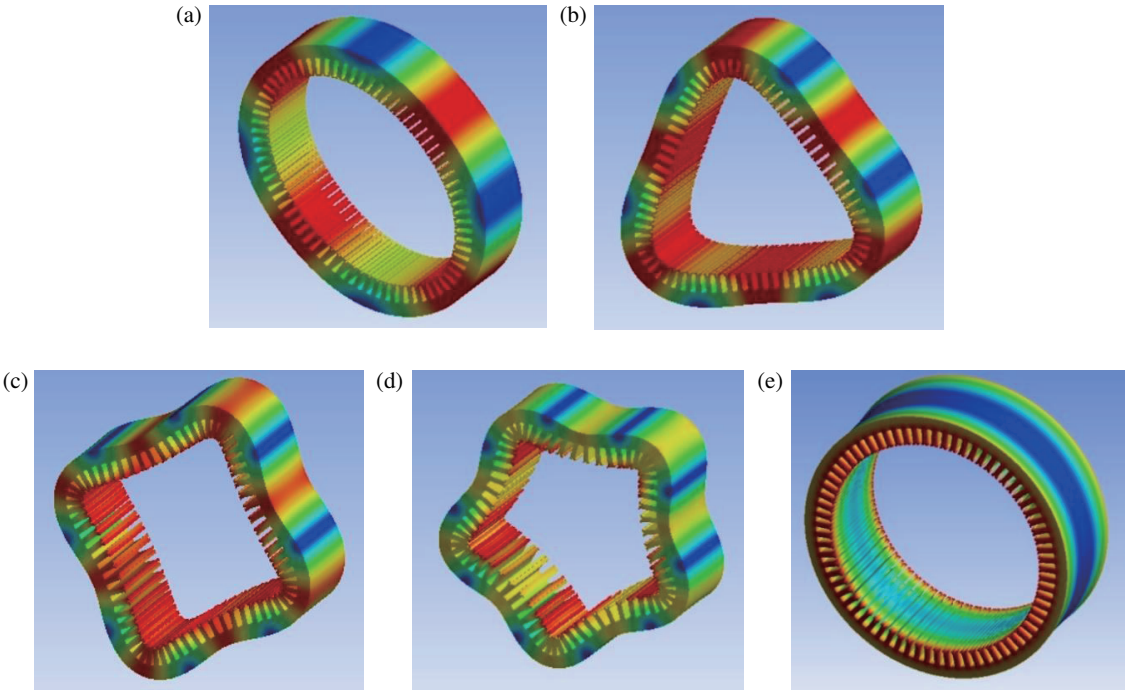

FIGURE 10. (a) 2nd-order mode (308.1 Hz). (b) 3rd-order mode (714.4 Hz). (c) 4th-order mode (1343.2 Hz). (d) 5th-order mode (1779.8 Hz). (e) 0th-order mode (2604.5 Hz).

tor. The lower the order of the radial electromagnetic force is, the greater the influence is on the vibration and noise of the motor. Therefore, for this kind of motor, this paper mainly studies the natural modes of 2nd to 5th order natural modes, and since the 1st order mode has a very low frequency and small influence, the 1st order mode is generally not analyzed. The modal shapes of the stator and the corresponding natural frequencies are shown in Figure 10. Since the fundamental frequency of the electromagnetic force of the motor studied in this paper is 200 Hz, the corresponding low-order frequencies of $2f$, $4f$, $6f$, and $8f$, namely 400 Hz, 800 Hz, 1200 Hz, and 1600 Hz are greatly different from the frequencies of the above-mentioned stator natural mode shapes, so it can be ensured that the resonance phenomenon will not occur.

The vibration acceleration spectra of the motor before and after slotting are shown in Figure 11. It can be found that the vibration acceleration amplitude under even frequency doubling is larger, and the vibration acceleration corresponding to $2f$ (400 Hz) is the largest. The maximum vibration acceleration after slotting is 150.58 mm/s^2, which is 33.44 mm/s^2 lower than that of the original motor (184.02 mm/s^2), and the optimization effect is obvious. The vibration acceleration corresponding to $4f$ (800 Hz), $6f$ (1200 Hz), $8f$ (1600 Hz) also decreases slightly. When the frequency reaches $13f$ (2600 Hz), it is very close to the natural frequency (2604.5 Hz) of the 0th-order mode of the motor stator. Therefore, the peak value at this point is larger than that at other points, but through the slotting design in this paper, the vibration acceleration of this point is also effectively reduced.

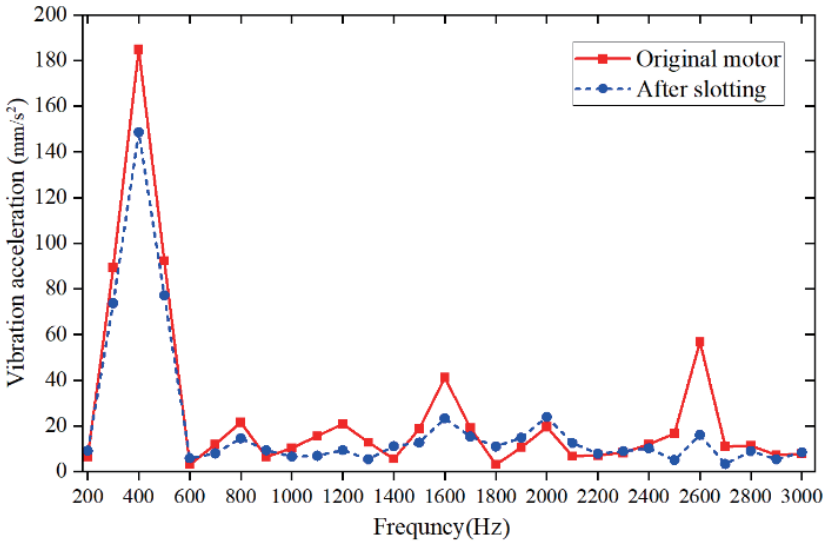

FIGURE 11. Vibration acceleration spectrum.

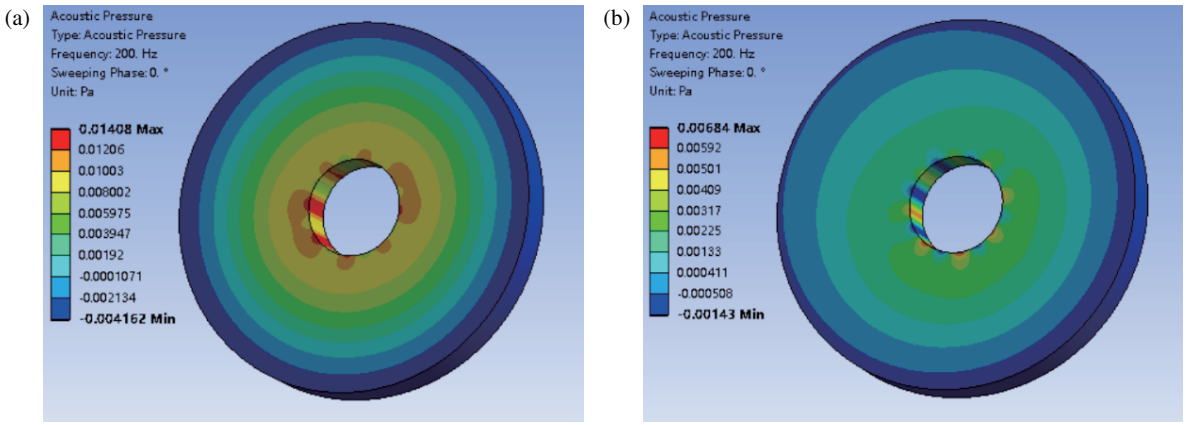

FIGURE 12. Sound pressure cloud diagram. (a) Original motor. (b) After slotting.

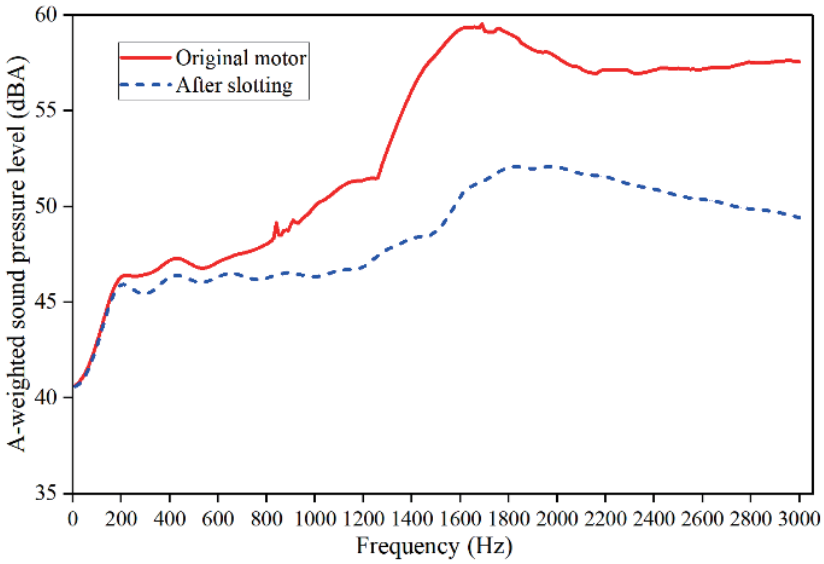

FIGURE 13. A-weighted sound pressure level spectrum.

The air domain 1 metre away from the circumference of the motor is selected as the test area for simulation, and based on the harmonic response analysis, the vibration acceleration is coupled to ANSYS Mechanical ACT as the excitation. The sound pressure cloud of the motor is obtained as shown in Figure 12. It can be seen that the maximum sound pressure value of the motor is changed from 0.01408 Pa to 0.00684 Pa, which is 51.42% lower. In order to better simulate the auditory characteristics of the human ear, the A-weighted sound pressure level is used to evaluate the noise response of the motor. It can be seen from Figure 13 that the A-weighted sound pressure level of the motor after slotting has different degrees of reduction in each frequency band. The average A-weighted sound pressure level is changed from 54.32 dBA to 48.55 dBA, a decrease of 5.77 dBA, and the peak A-weighted sound pressure level is changed from 59.76 dBA to 54.08 dBA, a decrease of 5.68 dBA. The effect of noise suppression is significant.

6. CONCLUSION

In this paper, a 72-slot 16-pole permanent magnet assisted synchronous reluctance motor with H315 frame number is taken as the research object. A slotting scheme with auxiliary slots in stator teeth and magnetic isolation holes in rotor is adopted to suppress the vibration and noise of the motor. The research results show that compared with the traditional method of only slotting the stator teeth or only opening the isolation holes to the rotor, this scheme has a better weakening effect on the amplitude of the radial electromagnetic force and the total harmonic distortion rate of the air gap flux density of the motor, which is more conducive to suppressing the vibration and noise of the motor. Finally, the multi-physical fields of the modal, vibration response, and noise response of the motor are analyzed. The results show that the maximum vibration acceleration of the motor is reduced by 33.44 mm/s^2, and the peak A-weighted sound pressure level of the motor decreases by 5.68 dBA, which verifies the rationality and effectiveness of the proposed method, and has certain reference value and engineering significance.

REFERENCES

[1] Di, C., X. H. Bao, J. Pan, and C. Y. Wang, "Modelling and analysis of a ferrite assisted synchronous reluctance machine based on the open-source platform Elmer," *Transactions of China Electrotechnical Society*, Vol. 37, No. 5, 1136–1144, 2022.

[2] Li, X., S. Wang, M. Yi, *et al.*, "Simulation analysis of NdFeB permanent magnet reluctance synchronous motor," *Small & Special Electrical Machines*, Vol. 46, No. 8, 49–51, 2018.

[3] Du, L., X. Liu, J. Fu, J. Liang, and C. Huang, "Design and optimization of reverse salient permanent magnet synchronous motor based on controllable leakage flux," *CES Transactions on Electrical Machines and Systems*, Vol. 5, No. 2, 163–173, Jun. 2021.

[4] Li, X. H., S. R. Huang, and L. Z. Li, "Calculation and analysis of vehicle vibration and noise of permanent magnet synchronous motor applied in electric vehicle," *Electric Machines and Control*, Vol. 17, No. 8, 37–42, 2013.

[5] Han, X., C. Li, X. Zhang, and S. Wang, "Quasi-analytical calculation of vibration and noise of permanent magnet assisted synchronous reluctance motor and analysis of its influencing factors," *Electric Machines and Control*, Vol. 193, No. 11, 5–12, 2020.

[6] Shi, J., Y. Hu, B. Chen, *et al.*, "Analysis and suppression of electromagnetic vibration in permanent magnet assisted synchronous reluctance motor," *Small & Special Electrical Machines*, Vol. 49, No. 6, 12–16, 2021.

[7] Ni, M., Y. Zuo, L. Liao, and Z. Yang, "Electromagnetic vibration analysis for permanent magnet synchronous motor," *Micromotors*, Vol. 48, No. 1, 7–11, 2015.

[8] Wang, K., H. Sun, L. Zhang, *et al.*, "An overview of rotor pole optimization techniques for permanent magnet synchronous machines," *Proceedings of the CSEE*, Vol. 37, No. 24, 7304–7317, 2017.

[9] Wang, X. Y., X. Y. He, and P. Gao, "Research on electromagnetic vibration and noise reduction method of V type magnet rotor permanent magnet motor electric vehicles," *Proceedings of the CSEE*, Vol. 39, No. 16, 4919–4926, 2019.

[10] Li, Q., S. Liu, and Y. Hu, "Vibration characteristics of permanent magnet motor stator system based on vibro-inertance matrix method," *IEEE Transactions on Energy Conversion*, Vol. 37, No. 3, 1777–1788, Sep. 2022.

[11] Huang, C., J. Duan, M. Zhou, *et al.*, "Analysis of reducing vibration of switched reluctance motor using new stator with slot on tooth tip," *Small & Special Electrical Machines*, Vol. 49, No. 8, 21–26, 2021.

[12] Han, X., X. Zhang, L. Zhu, *et al.*, "Measures to reduce vibration and noise of interior permanent magnet synchronous motor with multilayer permanent magnets," *Electric Machines and Control*, Vol. 25, No. 9, 2021.

[13] Xu, K., H.-L. Ying, S.-R. Huang, *et al.*, "Electromagnetic noise reduction of permanent magnet synchronous motor by step-skewed rotor," *Engineering Science*, Vol. 11, No. 53, 2248, 2019.

[14] Wang, X., X. Sun, and P. Gao, "Study on the effects of rotor-step skewing on the vibration and noise of a PMSM for electric vehicles," *IET Electric Power Applications*, Vol. 14, No. 1, 131–138, Jan. 2020.

[15] Tsoumas, I. P. and H. Tischmacher, "Influence of the inverter's modulation technique on the audible noise of electric motors," *IEEE Transactions on Industry Applications*, Vol. 50, No. 1, 269–278, 2014.

[16] Li, Q., S. Liu, W. Fang, X. Li, and Z. Tse, "Sideband vibration suppression of interior permanent magnet synchronous motors for electric vehicles under multiple operating conditions," *IEEE Transactions on Transportation Electrification*, Vol. 9, No. 1, 322–335, Mar. 2023.

[17] Lin, F., S. Zuo, W. Deng, and S. Wu, "Modeling and analysis of electromagnetic force, vibration, and noise in permanent-magnet synchronous motor considering current harmonics," *IEEE Transactions on Industrial Electronics*, Vol. 63, No. 12, 7455–7466, Dec. 2016.

[18] Ma, C. and S. Zuo, "Black-box method of identification and diagnosis of abnormal noise sources of permanent magnet synchronous machines for electric vehicles," *IEEE Transactions on Industrial Electronics*, Vol. 61, No. 10, 5538–5549, 2014.